International Journal of Materials Science and Applications
2025, Vol. 14, No. 3, pp. 79-88
https://doi.org/10.11648/j.ijmsa.20251403.14

Research Article

Influence of Window Layers on the Spectral Evolution of the Total Current Flowing Through a Solar Cell Based on Lead-Free Perovskite Materials

Saliou Seck*, Alioune Sow, Mamadou Salif Mane, Modou Faye, El Hadji Mamadou Keita, Amadou Ndiaye, Bachirou Ndiaye, Babacar Mbow, Cheikh Sene

Department of Physics, Faculty of Sciences and Technology, Semiconductors and Solar Energy Laboratory, Cheikh Anta Diop University, Dakar, Senegal

Abstract

In this work a modeling study of photovoltaic devices based on lead-free CH_3 NH_3 $Sn_{(1-y)}Ge_y$ I_3 perovskite materials, is carried out with different window layers. The transport window layers materials used are ZnO, TiO_2 and SnO_2. They enable minority charge carriers to be transported to the active perovskite layer and collected there. The study also focuses on the influence of geometric parameters such as the diffusion length of minority charge carriers, the surface recombination velocity and the thickness of the window layers on the performance of the devices. The photovoltaic devices have first been modeled using the ZnO window layer in the multijunction $ZnO(n^+)/Cu_2O(n)/CH_3NH_3Sn_{(1-y)}Ge_yI_3(p)$ structure. The ZnO window layer was then successively substituted by the TiO_2 and SnO_2 layers, leading thus to TiO_2 $(n^+)/Cu_2$ $O(n)/CH_3NH_3Sn_{(1-y)}Ge_yI_3(p)$ and SnO_2 $(n^+)/Cu_2$ $O(n)/$ CH_3 NH_3 $Sn_{(1-y)}Ge_y$ I_3 (p) photovoltaic structures, respectively. The CH_3 NH_3 $Sn_{(1-y)}Ge_y$ I_3 perovskite absorber layers considered in these structures contain a germanium content varying from 0 to 1. Our study showed that the best performances are obtained for a germanium content of around 0.25, corresponding to 65.8%, 49.7% and 64.5%, for ZnO, SnO_2 and TiO_2 window layers, respectively.

Keywords

Lead-Free Perovskite, Internal Quantum Efficiency, Solar Cell

1. Introduction

Progress in the field of solar cells is steadily increasing, driven by the world's strong demand for energy. Faced with this growing demand, solutions for efficient, low-cost, non-polluting and environmentally-friendly photovoltaic energy production systems have emerged. These include solar cells based on lead-free perovskite materials, which have the advantage of a direct band gap and thus a high absorption coefficient, which allows them to be used in thin-film solar cells. In addition, there are simple and accessible deposition techniques for these materials, which are synonymous with low cost.

Among the lead-free perovskite materials in use, mixed

*Corresponding author: saliou12.seck@ucad.edu.sn (Saliou Seck)

Received: 14 May 2025; **Accepted:** 28 May 2025; **Published:** 23 June 2025

tin-germanium perovskites have been the focus of recent work to improve device stability while maintaining high photovoltaic performance [1, 2]. The synthesis of mixed Sn-Ge perovskites, with the structure $CH_3NH_3Sn_{(1-y)}Ge_yI_3$ with $0 \le y \le 1$ [3], shows that the partial substitution of germanium (Ge) at the tin (Sn) site in $CH_3NH_3SnI_3$ perovskite up to 50% keeps the resulting materials in a tetragonal phase. At higher Ge content, transition from the tetragonal to a trigonal phase is observed [3]. According to these authors, the origin of this phenomenon is due to the large size difference between tin (Sn) and germanium (Ge) atoms [3]. Lead-free Sn-Ge mixed perovskites are direct bandgap semiconductors with bandwidth ranging from 1.38 eV to 2.0 eV, and are suitable for a wide range of applications, from light-emitting diodes to solar cells.

In thin film solar cells, window, buffer and absorber layers play an important role for photovoltaic efficiency. A wide bandgap window layer with low series resistance is essential for the operation of a solar cell.

In the present work we investigate the influence of window layers on the internal quantum efficiency of solar cells based on $CH_3NH_3Sn_{(1-y)}Ge_yI_3$ lead-free perovskite materials, with $0 \le y \le 1$. The window layers used are thin ZnO, TiO_2 and SnO_2 layers. These materials enable minority carriers to be collected and transported to the perovskite active layer. To do this, we first modeled our photovoltaic device with the ZnO layer in the $ZnO(n^+)/Cu_2O(n)/CH_3NH_3Sn_{(1-y)}Ge_yI_3(p)$ structure, then we successively substituted the ZnO layer with TiO_2 and SnO_2 window layers, getting $TiO_2(n^+)/Cu_2O(n)/CH_3NH_3Sn_{(1-y)}Ge_yI_3(p)$ and $SnO_2(n^+)/Cu_2O(n)/CH_3NH_3Sn_{(1-y)}Ge_yI_3(p)$ structures, respectively. The Cu_2O material acts as a buffer layer for all three models, ensuring also a good electrical contact and a good transition between the absorber and the various window layers considered.

2. Theoretical Approach and Modeling

The equations used to model solar cell operation are based on the continuity equations of the minority carriers in each part of the solar cell. These continuity equations make it possible to study all the phenomena that occur in semiconductors and to determine the parameters and properties of devices manufactured using these materials.

The space charge region is assumed to lie between the n-type Cu_2O and p-type $CH_3NH_3Sn_{(1-y)}Ge_yI_3$ layers. The electric field is also assumed to be zero outside this region. In the steady-state case, the continuity equations are given by:

$$\frac{1}{q} div\overrightarrow{J_n} + G_n - R_n = 0$$

$$-\frac{1}{q} div\overrightarrow{J_p} + G_p - R_p = 0$$

In the absence of an electric field, we can have:

$$\overrightarrow{J_n} = qD_n.\overrightarrow{grad}(n)$$

$$\overrightarrow{J_p} = -qD_p.\overrightarrow{grad}(p)$$

Our calculations are limited to the one-dimensional case. The solar cell model used in this work is illustrated in Figure 1.

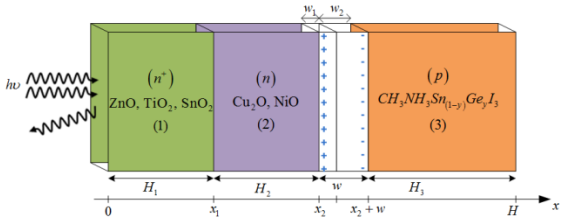

Figure 1. *$CH_3NH_3Sn_{(1-y)}Ge_yI_3$ perovskite solar cell Model.*

Its structure is (n^+) – Window layer/(n) – Buffer layer/(p) – $CH_3NH_3Sn_{(1-y)}Ge_yI_3$

The absorber material is the $CH_3NH_3Sn_{(1-y)}Ge_yI_3$ perovskite layer. It is a p-type semiconductor material whose main function is to absorb photons from incident solar radiation to generate electron-hole pairs.

One of the special features of this material is its bandgap width, which can be modulated according to its y germanium content.

The forbidden band width is 1.3 eV for $CH_3NH_3SnI_3$ $(y = 0)$ and 2.0 eV for $CH_3NH_3GeI_3$. Varying germanium content in the material makes it possible to continuously vary the band gap width between 1.3 eV and 2.0 eV.

The 50 nm thick n-type Cu_2O oxide layer, known as the buffer layer, is deposited on the $CH_3NH_3Sn_{(1-y)}Ge_yI_3$ perovskite surface. This n-type semiconductor layer provides the n-p junction with the absorber on one side and forms an interface with the ZnO window layer on the other side. Its bandgap width of about 2.1 eV and its non-toxicity, make Cu_2O one of the most promising materials for photovoltaic applications.

The transparent conductive oxide ZnO window layer completes the structure of the solar cell. It is first made up of a very thin intrinsic ZnO layer, about 50 nm thick, which serves

to cover the buffer layer and which also reduces short circuits in the device. It is then supplemented by the deposition of an aluminum-doped ZnO layer (ZnO: Al) with a thickness between 0.5 μm and 1μm.

Highly aluminum-doped ZnO layer has a high conductivity and is highly transparent. It allows incident photons to pass through to the absorber and also allows the collection of charge carriers due to its high conductivity.

2.1. Current Density Generated by Light in the Emitter

The holes current density $J_{ph,E}$ generated by the incident photons in the emitter comprises two contributions: the current density generated in the n+-window layer region, J_{ph_1} and the current density generated in the n-buffer region, J_{ph_2}.

$$J_{ph,E} = J_{ph_1} + J_{ph_2}$$

2.1.1. Current Density Generated in the n^+ - Region

In the ZnO window layer region where minority carriers are the holes, the continuity equation is given by:

$$\frac{d^2\Delta_{p_1}}{dx^2} - \frac{\Delta_{p_1}}{{L_{p_1}}^2} = -\frac{g_{ZnO}}{D_{p_1}}$$

$$g_{ZnO} = \alpha_{ZnO} F(1-R) e^{-\alpha_{ZnO} x} \text{ and } {L_{p_1}}^2 = D_{p_1}\tau_{p_1}$$

In this equation Δ_{p_1} is the minority carrier concentration, L_{p_1} and D_{p_1} are the hole diffusion length and the hole diffusion coefficient in the window layer region, respectively.

τ_{p_1} and α_{ZnO} represent the hole lifetime and absorption coefficient of the window layer, respectively.

R is the reflection coefficient and $F(E,\lambda)$ the incident photon flux of energy E and wavelength $\lambda(nm)$.

The resolution of this equation was made taking into account the following boundary conditions:

$$D_{p_1}\frac{\partial\Delta_{p_1}}{\partial x} = S_{p_1}\times\Delta_{p_1} \rightarrow \text{ for x = 0}$$

$$\Delta_{p_1} = 0 \rightarrow \text{ for x = } x_1$$

Where S_{p_1} is the recombination velocity on the front surface of the window layer.

The photocurrent J_{ph_1} in this region is given by:

$$J_{ph_1} = -qD_{p_1}\frac{\partial\Delta_{p_1}(x_1)}{\partial x}$$

$$J_{ph_1} = \frac{q\alpha_{ZnO}F(1-R)L_{p_1}}{\left(\alpha_{ZnO}{}^2 {L_{p_1}}^2 - 1\right)}\left\{\frac{\left(\frac{S_{p_1}L_{p_1}}{D_{p_1}} + \alpha_{ZnO}L_{p_1}\right) - e^{-\alpha_{ZnO}x_1}\left[\frac{S_{p_1}L_{p_1}}{D_{p_1}}ch\left(\frac{x_1}{L_{p_1}}\right) + sh\left(\frac{x_1}{L_{p_1}}\right)\right]}{\frac{S_{p_1}L_{p_1}}{D_{p_1}}sh\left(\frac{x_1}{L_{p_1}}\right) + ch\left(\frac{x_1}{L_{p_1}}\right)} - \alpha_{ZnO}L_{p_1}e^{-\alpha_{ZnO}x_1}\right\}$$

2.1.2. Current Density Generated in the n – Region

In this buffer layer region consisting in the thin n – type Cu_2O layer , minority carriers are also the holes. The continuity equation for these charge carriers is given by:

$$\frac{d^2\Delta_{p_2}}{dx^2} - \frac{\Delta_{p_2}}{{L_{p_2}}^2} = -\frac{g_{Cu_2O}}{D_{p_2}}$$

Where:

$$g_{Cu_2O} = \alpha_{Cu_2O}F(1-R)e^{-\alpha_{ZnO}x_1}.e^{-\alpha_{Cu_2O}(x-x_1)} \text{ and}$$

$${L_{p_2}}^2 = D_{p_2}\tau_{p_2}$$

Δ_{p_1} is the minority carrier concentration. L_{p_2} and D_{p_2} are the hole diffusion length and the hole diffusion coefficient in the buffer layer region, respectively.

τ_{p_2} and α_{Cu_2O} represent the hole lifetime and absorption coefficient of the buffer layer respectively.

Taking into account the boundary conditions defined as follows,

$$D_{p_2}\frac{\partial\Delta_{p_2}}{\partial x} = S_{p_2}\times\Delta_{p_2} + D_{p_1}\times\frac{\partial\Delta_{p_1}}{\partial x} \rightarrow \text{ x = } x_1$$

$$\Delta_{p_2} = 0 \rightarrow \text{ for x = } x_2$$

the photocurrent in the $x_1 \le x \le x_2$ region is given by:

$$J_{ph_2} = -qD_{p_2}\frac{\partial\Delta_{p_2}(x_2)}{\partial x}$$

$$J_{ph_2}=\frac{q\alpha_{Cu_2O}F(1-R)L_{p_2}e^{-\alpha_{ZnO}x_1}}{\left(\alpha_2{}^2L_{p_2}{}^2-1\right)}\left\{\frac{\left(\frac{S_{p_2}L_{p_2}}{D_{p_2}}+\alpha_{Cu_2O}L_{p_2}\right)-e^{-\alpha_{Cu_2O}(x_2-x_1)}\left[\frac{S_{p_2}L_{p_2}}{D_{p_2}}ch\left(\frac{x_2-x_1}{L_{p_2}}\right)+sh\left(\frac{x_2-x_1}{L_{p_2}}\right)\right]}{\frac{S_{p_2}L_{p_2}}{D_{p_2}}sh\left(\frac{x_2-x_1}{L_{p_2}}\right)+ch\left(\frac{x_2-x_1}{L_{p_2}}\right)}\right.$$

$$\left.-\alpha_{BL}L_{p_2}e^{-\alpha_{Cu_2O}(x_2-x_1)}\right\}$$

$$+\frac{J_{ph_1(x_1)}}{\frac{S_{p_2}L_{p_2}}{D_{p_2}}sh\left(\frac{x_2-x_1}{L_{p_2}}\right)+ch\left(\frac{x_2-x_1}{L_{p_2}}\right)}$$

2.2. Current Density Generated in the Space Charge Area

In the space charge layer, carrier recombination may be neglected. Indeed, it is assumed that the transit time of the free carriers in this zone is much shorter than their lowest lifetime because of the strong electric field which prevails therein. So, charge carriers will not have time to recombine and will all be collected.

In this region, the current density is given by:

$$J_{ZCE}=-qF(1-R)e^{-\alpha_{ZnO}x_1}e^{-\alpha_{Cu_2O}(x_2-x_1)}\left[e^{-\alpha_{Cu_2O}w_1}-1\right]-qF(1-R)e^{-\alpha_{ZnO}x_1}e^{-\alpha_{Cu_2O}\left[(x_2+w_1)-x_1\right]}\left[e^{-\alpha_{MASGI}w_2}-1\right]$$

2.3. Current Density Generated in the p – Type Region

In this region, the photo-current is an electron due current. The continuity equation for minority carriers (electrons) is given by:

$$\frac{d^2\Delta_{n_3}}{dx^2}-\frac{\Delta_{n_3}}{L_{n_3}{}^2}=-\frac{g_{MASGI}}{D_{n_3}}$$

Where:

$$g_{MASGI}=\alpha_{MASGI}F(1-R)e^{-\alpha_{ZnO}x_1}.e^{-\alpha_{Cu_2O}\left[(x_2+w_1)-x_1\right]}.e^{-\alpha_{MASGI}\left[x-(x_2+w_1)\right]}\ \text{ and }\ L_{n_3}{}^2=D_{n_3}\tau_{n_3}$$

Δ_{n_3} is the minority carrier concentration. L_{n_3} and D_{n_3} are the electron diffusion length and the electron diffusion coefficient in the absorber layer region, respectively.

τ_{n_3} represent the electron lifetime and α_{MASGI} the absorption coefficient of the absorber $CH_3NH_3Sn_{(1-y)}Ge_yI_3$ layer.

With boundary conditions defined as follows:

$$D_{n_3}\frac{\partial\Delta_{n_3}}{\partial x}=-S_{n_3}\times\Delta_{n_3}\ \rightarrow\ \text{for x = H}$$

$$\Delta_{n_3}=0\ \rightarrow\ \text{for x = x}_2+w$$

we get the following expression for the photocurrent in the absorber layer:

$$J_{ph_3}=qD_{n_3}\frac{\partial\Delta_{n_3}(x_2+w)}{\partial x}$$

$$J_{ph_3}=-\frac{q\alpha_{MASGI}F(1-R)L_{n_3}e^{-\alpha_{ZnO}x_1}e^{-\alpha_{BL}(x_2-x_1+w_1)}}{\left(\alpha_3{}^2L_{n_3}{}^2-1\right)}\times$$

$$\left\{\frac{\left(\alpha_{MASGI}L_{n_3}-\frac{S_{n_3}L_{n_3}}{D_{n_3}}\right)e^{-\alpha_{MASGI}\left[H-(x_2+w_1)\right]}+e^{-\alpha_{MASGI}w_2}\left[\frac{S_{n_3}L_{n_3}}{D_{n_3}}ch\left(\frac{H-(x_2+w)}{L_{n_3}}\right)+sh\left(\frac{H-(x_2+w)}{L_{n_3}}\right)\right]}{\frac{S_{n_3}L_{n_3}}{D_{n_3}}sh\left(\frac{H-(x_2+w)}{L_{n_3}}\right)+ch\left(\frac{H-(x_2+w)}{L_{n_3}}\right)}-\alpha_{MASGI}L_{n_3}e^{-\alpha_{MASGI}w_2}\right\}$$

2.4. Expression of the Total Photocurrent

The total photocurrent results from the contributions of the different parts of the cell. For a given wavelength, it represents, for our model, the sum of all the above calculated current components, which include the hole diffusion currents in the window and buffer regions, the current generated in the space charge region and the electron diffusion current in the p-type region.

$$J_{ph,T} = J_{ph,E} + J_{ZCE} + J_{ph_3}$$

The internal quantum efficiency is then given:

$$IQE = \frac{J_{ph,T}}{qF(1-R)}$$

The total current flowing through the solar cell was calculated using ZnO and Cu_2O absorption coefficients from [4, 5]. Those of the perovskite materials $CH_3NH_3Sn_{(1-y)}Ge_yI_3$ are obtained from S. Nagane et al. [3] and completed by S. Seck et al [6] for energy photons ranging from 0.8 eV to 3.5 eV to cover the entire visible spectrum.

3. Results and Discussion

The internal quantum efficiency (IQE) curves of the $ZnO(n^+)/Cu_2O(n)/CH_3NH_3Sn_{(1-y)}Ge_yI_3(p)$ photovoltaic device for different values of the germanium (Ge) content in the in the $CH_3NH_3Sn_{(1-y)}Ge_yI_3$ perovskite material, are shown in Figure 2. The diffusion lengths of minority carriers in regions 1 and 2 are set at 0.55 μm and 0.05 μm, respectively. The thicknesses of these regions being set at 0.55 μm and 0.05 μm, respectively. The thickness of the $CH_3NH_3Sn_{(1-y)}Ge_yI_3$ absorber is 0.5 μm while and the diffusion length of the minority carriers is evaluated at 0.5 μm.

For germanium contents in perovskite absorber layer between 0 and 0.25, the maximum internal quantum efficiency increases from 62.9% to 65.8%. For higher Ge contents, a gradual decrease in the maximum response is observed up to 52.6%, corresponding to zero Sn content in the absorber.

The internal quantum efficiency is higher for germanium content values of around 0.25, which correspond to perovskite layers with compositions close to that of $CH_3NH_3Sn_{0.75}Ge_{0.25}I_3$.

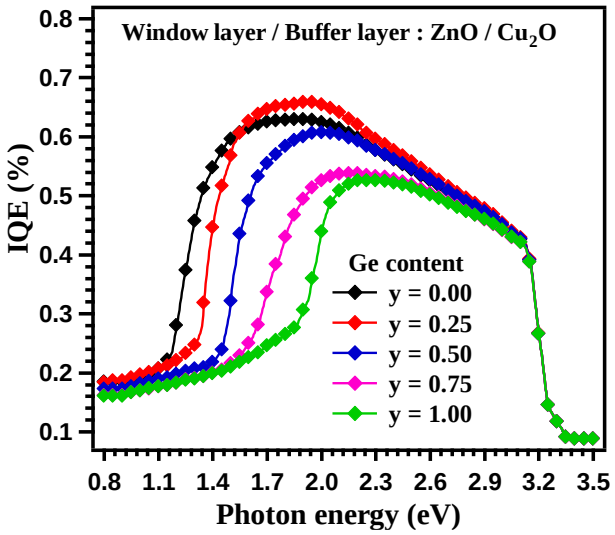

Figure 2. *Internal quantum efficiency of the* $ZnO(n^+)/Cu_2O(n)/CH_3NH_3Sn_{(1-y)}Ge_yI_3(p)$ *photovoltaic device as a function of photon energy for different Ge contents in the perovskite layer.*

In the rest of this part of the work, we focused on the study of the influence of the ZnO window layer on the internal quantum efficiency of the perovskite-based photovoltaic cell. To do this, we set the germanium content in the perovskite at 0.25 and, at the same time tried to optimize geometric parameters such as the diffusion length of minority carriers, the recombination velocity at the surface, the thicknesses of the layers, etc.

3.1. Influence of Minority Carrier Diffusion Length and Window Layer Thickness on Internal Quantum Efficiency

Figure 3 shows the quantum efficiency as a function of photon energy for different values of the minority carrier diffusion lengths in the ZnO window layer. The ZnO window layer thickness and the recombination velocity at the front surface are set at 0.55 μm and 2.10^7 $cm.s^{-1}$, respectively. The diffusion length was varied from 0.1 μm to 0.7 μm. Increasing the minority carrier diffusion length in the ZnO layer while maintaining a fixed thickness of 0.55 μm produces a slight impact on the total quantum efficiency of the solar cell. These low changes observed are mainly due to the fact that absorption in the ZnO layer corresponds to photons of short wavelength (high energy).

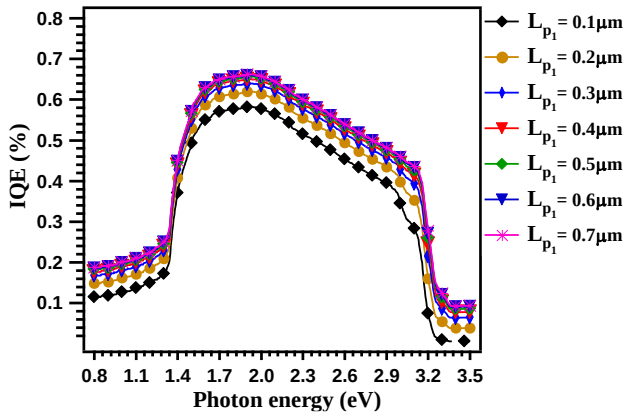

Figure 3. *Influence of the minority carrier diffusion length in the* ZnO *window layer on the internal quantum efficiency of the solar cell.*

For energies below the bandwidth of the ZnO window layer, losses in the photovoltaic cell can be influenced factors including variation in the diffusion length of minority carriers and sub-band absorption. In fact, photons with energies below the bandwidth can be absorbed by defect states or impurities in the ZnO layer.

Since the reduction of the minority carrier diffusion length is known to increase the probability of non-radiative recombination, it decreases thus the collection efficiency of charge carriers.

In order to obtain more qualitative information, we have investigated the effects of the absorber layer thickness on the device quantum efficiency. Figure 4 shows the variation of the internal quantum efficiency of the photovoltaic cell with photon energy for different values of the window layer thickness. The minority carrier diffusion length and the recombination velocity at the front side of the device are set at 0.55 µm and 2.10^7 $cm.s^{-1}$, respectively.

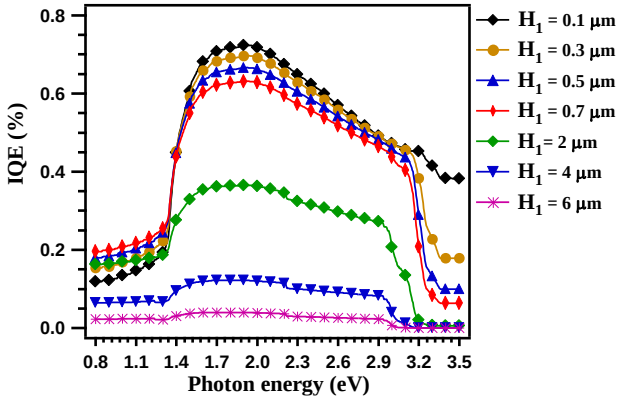

Figure 4. *Influence of* ZnO *window layer thickness on the internal quantum efficiency of the solar cell.*

As the thickness of the window layer increases, a decrease is observed in the efficiency of the cell. For thickness values of the window layer less than the diffusion length of the minority carriers, there is an improvement in the internal quantum efficiency, from 70% to 80%. Beyond thickness values above 0.7 µm, the device response drops drastically to very low values. Indeed, when the diffusion length of the minority carriers is small compared to the thickness of the window layer, most of the charge carriers created by photon absorption in this region cannot diffuse to the junction to be collected there.

Increasing the thickness of the ZnO window layer can lead to more absorption of the incident light before it reaches the active junction to generate charge carriers. This highly reduced transmission of photons through thicker ZnO layers limits the efficiency of the photovoltaic conversion. In addition, a thicker ZnO layer can, on the one hand, introduce more defects or impurities into the layer, increasing thus recombination losses of charge carriers, and on the other hand, modify the electrical properties of this layer by probably increasing the series resistance, which also contributes to reduce the overall efficiency of the cell. Increasing thickness can also lead to changes in the optical parameters such as the refractive index of the layer. These factors must be carefully optimized to maximize the internal quantum efficiency of the cell while minimizing losses.

The recombination velocity at the front surface of a ZnO window layer based-photovoltaic cell plays a crucial role in the overall performance of the device. In Figure 5, the recombination velocity S_{p_1} at the front surface of the window layer is varied from 2.101 cm. s^{-1} to 2.107 cm. s^{-1}. High front surface recombination velocities limit the ability of light-generated charge carriers to reach the junction and contribute electrical current, because of their low lifetime. Reduction of the photovoltaic conversion efficiency is then observed at high recombination rates as highlighted in Figure 5. At low recombination velocities, the contribution of the window layer to the internal quantum efficiency increases significantly.

To improve device's performance, it is essential to reduce the recombination velocity by optimizing the ZnO layer properties such as its crystalline qualities, and by surface treatment in order to reduce the defects or impurities present therein.

In figures 3, 4 and 5, we set the hole diffusion length in the Cu_2O layer at 0.5 µm while the thickness of this layer is set at 0.05 µm. The electron diffusion length in the $CH_3NH_3Sn_{0.75}Ge_{0.25}I_3$ absorber layer is 0.5 µm and the thickness the layer is 0.5 µm.

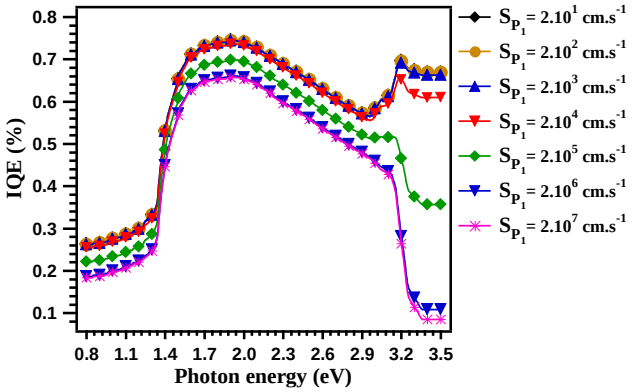

Figure 5. *Evolution of internal quantum efficiency as a function of photon energy for different values of recombination velocity at the front face.*

3.2. Influence of the Nature of Window Layer

TiO_2 and SnO_2 materials are also often used as window layers in thin-film photovoltaic devices because of their optical and electric properties. In this section, analysis of the influence of the nature of the window layer in the $CH_3NH_3Sn_{(1-y)}Ge_yI_3$ perovskite-based photovoltaic device is carried out by replacing the ZnO window layer by TiO_2 and then by SnO_2 window layer. TiO_2 and SnO_2 have band gap energies of 3.2 eV and 3.5 eV, respectively. Their absorption coefficients were taken from Zhang et al. [4] and Kar et al. [5].

3.2.1. TiO_2-Based Device

Figure 6 shows the spectral evolution of the total current flowing through the $TiO_2\left(n^+\right)/Cu_2O(n)/CH_3NH_3Sn_{(1-y)}Ge_yI_3(p)$ -based solar cell device for different values of the germanium content in the perovskite layer. The thickness layer and the minority carrier diffusion length in the TiO_2 used for calculations are both 0.55 μm. For the Cu_2O layer, the thickness is set at 0.05 μm and the diffusion length of minority carrier at 0.5 μm. The carrier diffusion length and thickness of the perovskite layer are both set at 0.5 μm.

A significant change is observed in the shape of the quantum efficiency variation curves of the devices. The values displayed by the quantum efficiency are lower than those obtained with the ZnO window layer. In the photon energy range below the bandgap width of the absorber, the quantum efficiency increases very slightly with the energy of the photons up to a maximum response which corresponds to the band gap energy of the corresponding $CH_3NH_3Sn_{(1-y)}Ge_yI_3$ absorber layer. Since increasing the germanium content in the absorber layer increases the bandgap energy of this latter, the maximum in the quantum efficiency is shifted towards higher energies. For photon energy values greater than 2 eV, the quantum efficiency retains almost the same value whatever the germanium content in the absorber and decreases monotonically to very low values.

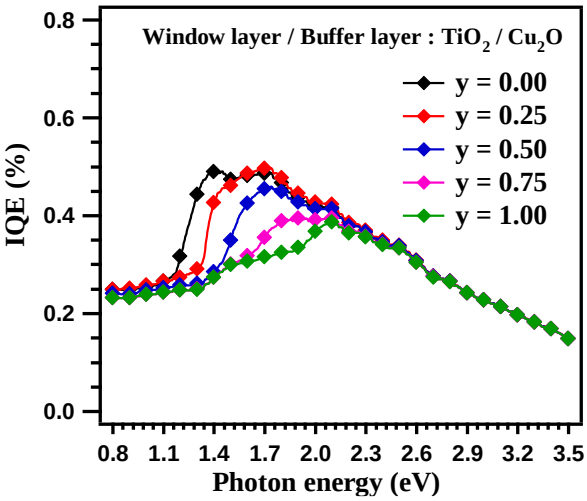

Figure 6. *Internal quantum efficiency as a function of photon energy for different y values for TiO_2 window layer.*

The maximum internal quantum efficiency improves from 49.1% for y = 0 $\left(E_g = 1.3\ eV\right)$ to 49.7% for y = 0.25 $\left(E_g = 1.43\ eV\right)$. Beyond y = 0.25, it decreases to 46% for y = 0.50 $\left(E_g = 1.67\ eV\right)$, 39.4% for y = 0.75 $\left(E_g = 1.76\ eV\right)$ and 38.7% for y = 1 $\left(E_g = 2\ eV\right)$. The best internal quantum efficiency corresponds to a value of y = 0.25, as obtained with ZnO and TiO_2 transport layers.

The best performances obtained for a germanium content of 0.25 can be explained on the one hand, by the fact that the layers corresponding to this value have a forbidden bandwidth closer to the theoretical optimum of the absorber materials in use for photovoltaic cells, and on the other hand because $CH_3NH_3Sn_{0.75}Ge_{0.25}I_3$ has absorption coefficients higher than those layers with the other germanium content values.

For Ge contents in the perovskite layer equal to or greater than 50%, the forbidden bandwidth of the materials is larger than the theoretical optimum. In addition, the phase transitions observed in the crystallographic structure of the material for these germanium content values [3, 7], make the perovskite unstable and degrade the performance of the solar cell.

Effect of the Minority Carrier Diffusion Length and TiO_2 Window Layer Thickness

Figure 7 shows the influence of the minority carrier diffusion length on the quantum efficiency of the device with TiO_2 as window layer. The TiO_2 thickness layer and the recombination velocity at the front surface are set at 0.55 μm and 2.10^7 cm.s^{-1}, respectively while the diffusion length varies from 0.1 μm to 0.7 μm. The minority carrier diffusion

length and the thickness of the perovskite layer are both set at 0.5 μm. The Cu_2O layer thickness is 0.05 μm and the minority carrier diffusion length 0.5μm.

An increase in the diffusion length of minority carriers in the window layer increases the contribution of this latter to the quantum efficiency. However, greater rates of variations are observed compared to the device using a ZnO window layer. This is probably due to greater optical losses on the front surface and to greater sub-band absorption in the of the window layer. In addition, TiO_2 has a lower electrical conductivity than ZnO, which may further limit the quantum efficiency of TiO_2-based devices.

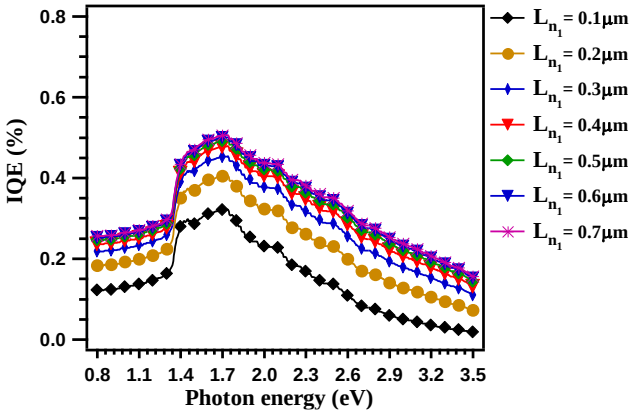

Figure 7. *Influence of the minority carrier diffusion length on the internal quantum efficiency of the device with TiO_2 as window layer.*

Figure 8 shows the internal quantum efficiency as a function of photon energy for different values of the thickness of the TiO_2 window layer. The diffusion length is set at 0.55 μm and the thickness is varied between 0.1 μm and 6 μm. For the Cu_2O and perovskite layers, the same values of thickness and diffusion lengths as those in Figure 8 have been retained.

As in the case of ZnO based window layer, increasing the thickness of the TiO_2 layer produces a rapid degradation in the quantum efficiency of the device.

This rapid deterioration in the device's performance reflects the fact that the loss phenomena identified in the case of the devices using the ZnO window layer are greater in the case of TiO_2, further showing that a very thin window layer is sufficient to improve the quantum efficiency of the solar cell.

3.2.2. SnO_2-based Device

As in the case of ZnO and TiO_2 window layers, Figure 9 shows the spectral evolution of the total current through the solar cell as a function of photon energies for different values of the germanium content in the $CH_3NH_3Sn_{(1-y)}Ge_yI_3$ perovskite material. The minority carrier diffusion length in the SnO_2 layer as well as the thickness of the latter are both set at 0.55μm. For the Cu_2O layer, the diffusion length of minority carriers is 0.5μm while the thickness is 0.05μm.

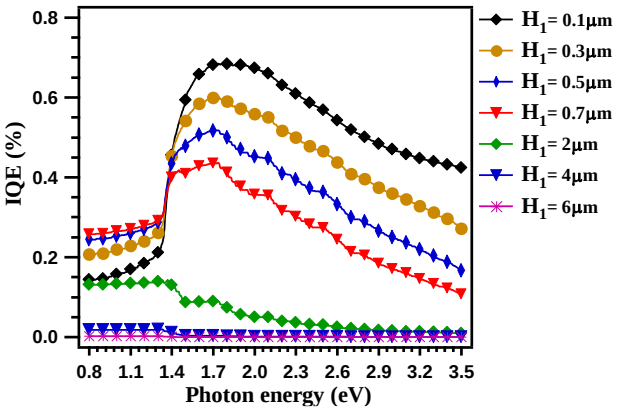

Figure 8. *Influence of TiO_2 layer thickness on internal quantum efficiency.*

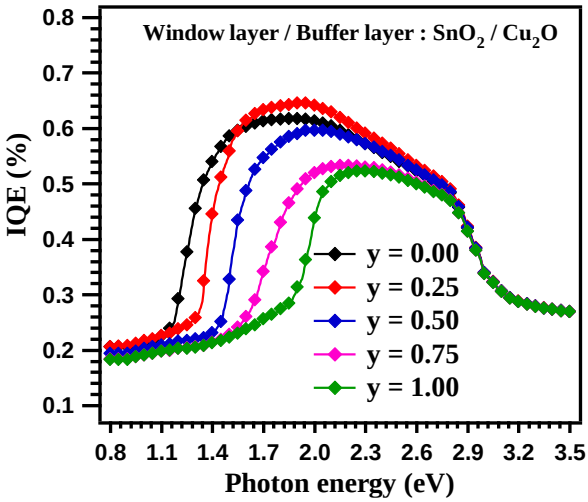

Figure 9. *Internal quantum efficiency as a function of photon energy for different Ge content in the perovskite for SnO_2 window layer-based device.*

The diffusion length of minority carriers and the thickness of the perovskite layer are also both set at 0.5μm.

The quantum efficiency first increases with photon energies up to a value corresponding to the bandgap width of the $CH_3NH_3Sn_{(1-y)}Ge_yI_3$ absorber layer. The variation of the germanium content in the perovskite material increases the band gap energy of the absorber, shifting therefore the maximum response to higher energies.

Above the band gap energy of the absorber, the quantum efficiency decreases to a value lower than 50%, at a photon energy of about 2.9 eV. Beyond this energy value the quantum efficiency continues to fall, keeping an almost identical value regardless of the germanium content in the $CH_3NH_3Sn_{(1-y)}Ge_yI_3$ perovskite layers.

The maximum internal quantum efficiency improves from 61.8% for y = 0 $(E_g = 1.3\ eV)$ to 64.5% for y = 0.25 $(E_g = 1.43\ eV)$. Beyond y = 0.25, the internal quantum efficiency decreases to 59.7% for y = 0.50 $(E_g = 1.67\ eV)$, 53.3% for y = 0.75 $(E_g = 1.76\ eV)$ and 52.2% for y = 1 $(E_g = 2\ eV)$. The best quantum efficiency corresponds to y = 0.25, i.e. with the $CH_3NH_3Sn_{0.75}Ge_{0.25}I_3$ absorber as with the ZnO and TiO_2 window layers.

Effect of Minority Carrier Diffusion Length and SnO_2 Window Layer Thickness

Figure 10 shows the influence of the minority carrier diffusion length on the internal quantum efficiency of the $SnO_2(n^+)/Cu_2O(n)/CH_3NH_3Sn_{0.75}Ge_{0.25}I_3(p)$ device as a function of photon energy. The SnO_2 layer thickness is 0.5 μm and the diffusion length is varied between 0.1 μm and 0.7 μm. We maintained the same values for minority carrier diffusion length and thicknesses of Cu_2O and $CH_3NH_3Sn_{0.75}Ge_{0.25}I_3$ layer.

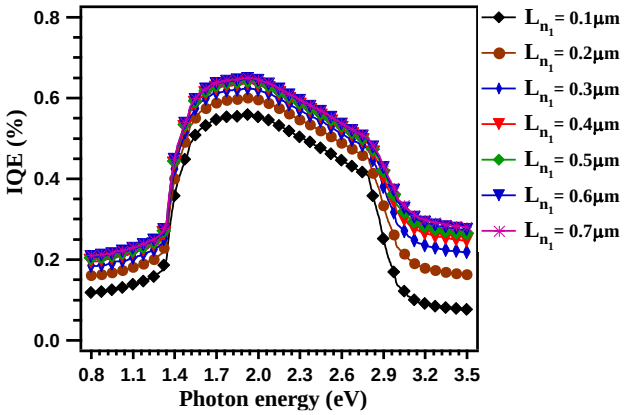

Figure 10. *Influence of the minority carrier diffusion length on internal quantum efficiency as a function of energy SnO_2 window layer-based device.*

We find that increasing the minority carrier diffusion length in SnO_2 from 0.1 μm to 0.7 μm slightly improves the maximum quantum efficiency up to a value of 65%.

Figure 11 shows the spectral evolution of the total current for different values of the SnO_2 layer thickness. The thickness of the SnO_2 layer is varied from 0.1 μm to 6 μm while the minority carrier diffusion length in this layer is kept at a constant value of 0.5 μm.

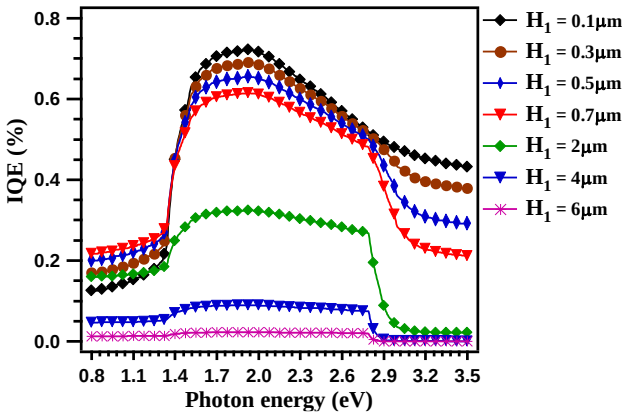

Figure 11. *Influence of SnO2 thickness on the internal quantum efficiency as a function of energy: SnO_2 window layer.*

It is noted that for the low thicknesses of the SnO_2 layer, the quantum efficiencies are better, reaching the maximum value of 72% for H = 0.1 μm.

Figure 12 shows the comparative study of the internal quantum efficiencies of the three photovoltaic devices. It highlights the best performances of the devices using ZnO and SnO_2 as window layers. The internal quantum efficiency reaches the maximum values of 65.8%, 64.5% and 49.7% for ZnO, SnO_2 and TiO_2 window layers, respectively.

In the 0.8-1.37 eV energy range, quantum efficiencies are very low with the $TiO_2(n^+)/Cu_2O(n)/CH_3NH_3Sn_{0.75}Ge_{0.25}I_3(p)$ device showing slightly better performances than the $ZnO(n^+)/Cu_2O(n)/CH_3NH_3Sn_{0.75}Ge_{0.25}I_3(p)$ and $SnO_2(n^+)/Cu_2O(n)/CH_3NH_3Sn_{0.75}Ge_{0.25}I_3(p)$ devices. The relative quantum efficiency variation in this region can be explained by the reflection phenomena at the front surface of the ZnO, TiO_2 and SnO_2 windows layers of the photovoltaic devices.

In the 1.37-1.74 eV energy range, the quantum efficiency of the TiO_2 based device reaches a maximum value of 49.7% while the ZnO and SnO_2 based devices have maximum quantum efficiencies of 65.8% and 64.5%, respectively. The lower quantum efficiency of the TiO_2 based device could be due to larger reflections at the TiO_2/Cu_2O interface, which could contribute to a sharp reduction in the number of photons reaching the active material. Above 1.74 eV, the internal quantum efficiency drops to low values. In the $(1.74\ eV \le E \le 2.80\ eV)$ energy range, $ZnO(n^+)/Cu_2O(n)/CH_3NH_3Sn_{0.75}Ge_{0.25}I_3(p)$ and $SnO_2(n^+)/Cu_2O(n)/CH_3NH_3Sn_{0.75}Ge_{0.25}I_3(p)$ devices show almost identical responses, but larger than that of $TiO_2(n^+)/Cu_2O(n)/CH_3NH_3Sn_{0.75}Ge_{0.25}I_3(p)$ device. At photon energies above 2.8 eV, the quantum efficiency of

$SnO_2(n^+)/Cu_2O(n)/CH_3NH_3Sn_{0.75}Ge_{0.25}I_3(p)$ device drops further while this behavior occurs in the $ZnO(n^+)/Cu_2O(n)/CH_3NH_3Sn_{0.75}Ge_{0.25}I_3(p)$ device from 3 eV. This behavior occurs due to reduced absorption at long wavelengths and due to recombination phenomena on the back surface of these devices.

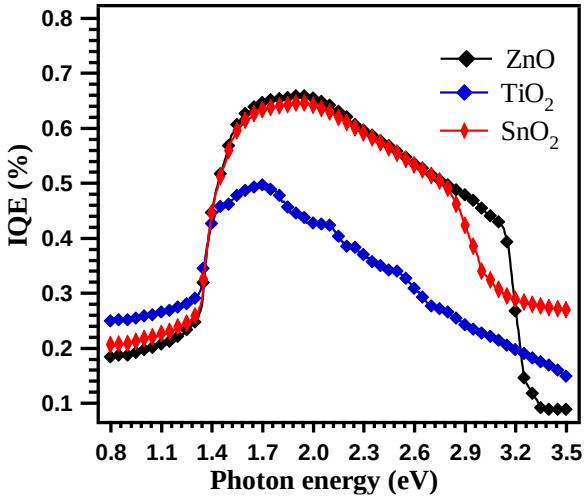

Figure 12. Internal quantum efficiency as a function of photon energy for the three devices.

4. Conclusion

In this work, we have carried out a theoretical study of the internal quantum efficiency of photovoltaic devices using the $CH_3NH_3Sn_{(1-y)}Ge_yI_3$ lead-free perovskite material as absorber. The study investigated also the influence of geometric parameters such as the minority diffusion length, the recombination velocity and the thickness of the ZnO, TiO_2 and SnO_2 window layers on the photovoltaic performances, by determining the spectral evolution of the total current. The three devices investigated in this study are $ZnO(n^+)/Cu_2O(n)/CH_3NH_3Sn_{(1-y)}Ge_{(y)}I_3(p)$, $TiO_2(n^+)/Cu_2O(n)/CH_3NH_3Sn_{(1-y)}Ge_{(y)}I_3(p)$ and $SnO_2(n^+)/Cu_2O(n)/CH_3NH_3Sn_{(1-y)}Ge_{(y)}I_3(p)$, respectively. The absorber layer based on $CH_3NH_3Sn_{(1-y)}Ge_yI_3$ perovskite material was considered for germanium content varying between 0 and 1. By analytically solving the continuity equations governing the minority carriers, we calculated the total current density flowing through each device. This allowed us to deduce the internal quantum efficiency of each device as a function of photon energies. The quantum efficiency of the $ZnO(n^+)/Cu_2O(n)/CH_3NH_3Sn_{0.75}Ge_{0.25}I_3(p)$, $TiO_2(n^+)/Cu_2O(n)/CH_3NH_3Sn_{0.75}Ge_{0.25}I_3(p)$ and $SnO_2(n^+)/Cu_2O(n)/CH_3NH_3Sn_{0.75}Ge_{0.25}I_3(p)$ devices showed maximum values of 65.8%, 49.7% and 64.5%, respectively and highlighted then the best performances of the ZnO window layer based device.

Abbreviations

IQE	Internal Quantum Efficiency
Ge	Germanium
Sn	Tin
MASGI	$CH_3NH_3Sn_{(1-y)}Ge_yI_3$

Conflicts of Interest

The authors declare no conflicts of interest.

References

[1] M. G. Ju, J. Dai, L. Ma, X. C. Zeng, Lead-free mixed tin and germanium perovskites for photovoltaic application, J. Am. Chem. Soc., 139 (2017) 8038−8043.

[2] P. Cheng, T. Wu, J. Liu, W. Q. Deng, K. Han, Lead-free, two-dimensional mixed germanium and tin perovskites, J. Phys. Chem. Lett., 9 (2018) 2518−2522.

[3] S. Nagane, D. Ghosh, R. L. Z. Hoye, B. Zhao, S. Ahmad, A. B. Walker, M. S. Islam, S. Ogale, A. Sadhanala, Lead-free perovskite semiconductors based on germanium-tin solid solutions: Structural and optoelectronic properties, J. Phys. Chem. C, 122 (2018) 5940−5947.

[4] L. Zhang, W. Liang, How the structures and properties of twodimensional layered perovskites MAPbI3 and CsPbI3 vary with the number of layers, J. Phys. Chem. Lett., 8 (2017) 1517-1523.

[5] M. Kar, R. Sarkar, S. Pal, P. Sarkar, Lead Free Two-Dimensional Mixed Tin and Germanium Halide Perovskites for Photovoltaic Applications, J. Phys. Chem., 125 (2021) 74−81.

[6] S. Seck, A. Sow, M. S. Mané, A. Ndiaye, E. M. Keita, B. Ndiaye, B. Mbow, and C. Sène, Modeling and Analysis of a Mixed Sn-Ge Lead Free Perovskite Based Solar Cells, American Journal of Energy Research, 12 (1) (2024) 1-7.

[7] Z. Shi, J. Guo, Y. Chen, Q. Li, Y. Pan, H. Zhang, Y. Xia, W. Huang, Lead-free organic-inorganic hybrid perovskites for photovoltaic applications: Recent advances and perspectives, Adv. Mater., 29 (2017) 1605005.